Journal of
Composites Science

MDPI

Article

A Green Approach to Surface Modification of Cellulose Nanocrystals via Grafting of Poly(2-hydroxyethyl methacrylate) and Development of Polybutylene–Adipate–Terephthalate-Based Nanocomposites

Eda Jan Yılmaz Arıkan [1], Yonca Alkan Göksu [1], Aylin Altınbay [2], Emre Vatansever [3], Sezer Enes Acar [1], Yusuf Ziya Bidiş [1] and Mohammadreza Nofar [1,4,*]

[1] Sustainable & Green Plastics Laboratory, Metallurgical & Materials Engineering Department, Faculty of Chemical and Metallurgical Engineering, Istanbul Technical University, Istanbul 34469, Turkey; arikan23@itu.edu.tr (E.J.Y.A.); alkanyo@itu.edu.tr (Y.A.G.); sezerenesacarr@gmail.com (S.E.A.); bidis21@itu.edu.tr (Y.Z.B.)
[2] Metallurgical & Materials Engineering Department, Faculty of Chemical and Metallurgical Engineering, Yildiz Technical University, Esenler, Istanbul 34220, Turkey; aylin.altinbay@yildiz.edu.tr
[3] Chemical Engineering Department, Polytechnique Montreal, Montreal, QC H3T 1J4, Canada; emrevtnsvr@gmail.com
[4] Mechanical Engineering Department, University of Alberta, Edmonton, AB T6G 2R3, Canada
* Correspondence: nofar@itu.edu.tr

Abstract

Cellulose nanocrystals (CNCs) possess outstanding mechanical properties and sustainability; however, their hydrophilic nature makes their dispersion challenging in hydrophobic bioplastic matrices. Surface modification of CNC is therefore inevitable for effective nanocomposite fabrication. In this study, CNC surface was modified using a green, water-based grafting-from method, enabling the growth of poly(2-hydroxyethyl methacrylate) (PHEMA) chains directly from its surface. This modification decreases intermolecular hydrogen bonding among CNCs and enhances their compatibility with poly(butylene adipate-co-terephthalate) (PBAT), a commercially available biodegradable aliphatic–aromatic copolyester widely used in sustainable packaging applications. The enhanced interfacial interaction arises from both the improved dispersion of CNCs within the PBAT matrix and the ability of PHEMA's hydroxyl groups to form secondary interactions with PBAT. To examine how grafted polymer chain length influences CNC dispersion, PHEMA was grown from CNC surfaces at different grafting degrees. Additionally, PHEMA homopolymers were synthesized and melt-mixed with PBAT to evaluate the role of PHEMA in the absence of CNC. Neat and modified CNCs (mCNCs) were characterized by Fourier transform infrared spectroscopy, X-ray diffraction, water contact angle measurements, wettability tests, and thermogravimetric analysis. Nanocomposites containing 3 wt% neat CNCs, mCNCs, or PHEMA homopolymers were subsequently prepared using an internal melt mixer. Melt rheology, differential scanning calorimetry, and dynamic mechanical analysis were then used to characterize the final viscoelastic and thermomechanical behavior of the resulting nanocomposites. The increased storage modulus and complex viscosity of the nanocomposites confirmed that the CNCs grafted with an intermediate PHEMA chain length exhibited improved network formation and enhanced interfacial interaction with PBAT.

Keywords: cellulose nanocrystals; surface modification; PHEMA; PBAT; rheology

Check for updates

Academic Editor: Salim Hiziroglu

Received: 31 December 2025
Revised: 25 February 2026
Accepted: 2 March 2026
Published: 5 March 2026

Copyright: © 2026 by the authors. Licensee MDPI, Basel, Switzerland. This article is an open access article distributed under the terms and conditions of the Creative Commons Attribution (CC BY) license.

1. Introduction

Increasing environmental awareness has accelerated the demand for biodegradable polymers and composites in consumer applications [1]. Cellulose, a natural high-molecular weight polymer mainly derived from wood and cotton [2], has emerged as a valuable raw material owing to its abundance, renewability, biodegradability, non-toxicity, and cost-effectiveness [3]. Among cellulose-derived materials, cellulose nanocrystals (CNCs) are rod-shaped, highly crystalline nanoparticles obtained through the acid hydrolysis of cellulose fibers. CNCs exhibit exceptional stiffness, low density, and high surface reactivity [4–10]. The dimensions and crystallinity of CNCs vary depending on the source material, with CNCs generally exhibiting widths of 5–10 nm and lengths of 50–500 nm [2]. Their high aspect ratio, low density (~1.6 g/cm^3), bending strength (~10 GPa), Young's modulus (~150 GPa) and tensile strength (~7.5 GPa) make them particularly suitable as reinforcement in biodegradable nanocomposites [11–13].

Nanocomposites containing CNCs can be produced using solution casting or melt-mixing methods [14,15]. Solution casting is straightforward and could promote enhanced CNC dispersion within different biopolymers like polylactide (PLA) and polybutylene adipate terephthalate (PBAT) by improvements in the rheological and thermal behaviors of nanocomposites [16–20]. Ozdemir et al. [21] showed that, among various solvents, DMF, and more specifically, DMSO, exhibited superior dispersion efficiency, yielding lower rheological percolation thresholds for CNCs, with values as low as ~1.52 wt.% and 0.12 wt.%, respectively. A lower rheological percolation threshold indicates that CNCs are able to form a continuous network within the polymer matrix at much lower filler loadings, showing improved dispersion quality and stronger particle–polymer interactions. However, residual solvent may suppress the mechanical properties, and the approach is not practical for scalable production [16,18,22]. Melt mixing could provide a scalable and solvent-free processing route that also prevents the mechanical property losses commonly associated with residual solvent contamination [14]. However, despite these advantages, neat CNCs tend to agglomerate under melt-processing conditions due to strong intermolecular hydrogen bonding and limited compatibility with hydrophobic polymer matrices [3,23]. Employing a hybrid processing strategy that combined solution casting and melt mixing, Bagheriasl et al. [24] investigated the rheological behavior of PLA containing 4 wt% CNC. Three preparation routes were compared: solution casting, direct melt mixing, and dilution of a solution-casted PLA/CNC masterbatch through melt mixing. Their results demonstrated that solution casting produced the most effective CNC dispersion, which translated into markedly enhanced rheological properties. In contrast, directly melt-mixed nanocomposites showed no significant improvement, while the dilution approach yielded intermediate performance—better than direct melt mixing but still below the solution-casted samples. The authors attributed this trend to the re-agglomeration of initially well-dispersed CNCs during the melt-mixing step, a consequence of strong particle–particle interactions. Similar trends were observed in a study conducted by Arslan et al. [16] in which PLA/CNC nanocomposites containing 1, 3, and 5 wt% CNC were produced via (a) solution casting using DMF and (b) dilution of a solution-casted masterbatch through melt mixing in a twin-screw extruder (TSE). In the nanocomposites prepared through solution casting, the CNC percolation network was established at CNC loadings between 1 and 3 wt%. However, in the melt-processed nanocomposites, the onset of solid network formation shifted to concentrations above 5 wt% CNC due to poorer dispersion and stronger nanoparticle agglomeration. Even CNCs that were initially well-dispersed in a solution casting masterbatch tended to re-agglomerate during subsequent melt mixing, preventing uniform dispersion.

The major challenge in producing CNC-based nanocomposites through melt-mixing strategies is their intrinsically hydrophilic nature [10,25]. Therefore, to enable the fabrication of CNC-containing nanocomposites through scalable melt-mixing processes, the CNC surface must be modified to suppress hydrogen-bond-driven agglomeration, especially in hydrophobic polymers [4,26–28]. Such modifications can be accomplished via physical adsorption, covalent functionalization, small-molecule grafting, or polymer grafting methods [25,26]. Notably, polymer grafting is particularly effective for CNC modification since it could offer control over polymer growth directly from the CNC surface [29].

Zhang et al. [30] grafted poly(butylene succinate) (PBS) onto CNC (PBS-*g*-CNC) in situ and incorporated it into a PBS/PLA (30/70) blend with dicumyl peroxide as a compatibilizer. PBS-*g*-CNC significantly improved the blend's morphology, crystallization behavior, and mechanical properties. In a study conducted by Rosli et al. [31], incorporating polymethylmethacrylate-grafted cellulose (Cell-*g*-PMMA) into polylactic acid/natural rubber blends enhanced tensile strength by up to 60%, with the highest improvement observed at 7.5 wt% loading. Spinella et al. [32] also synthesized the CNC-*g*-PMMA through radical polymerization techniques and produced PLLA nanocomposites containing 5 wt% unmodified CNC and CNC-*g*-PMMA by twin-screw extrusion followed by injection molding. Melt-state rheology showed that PMMA grafting significantly improved CNC dispersion with a percolation threshold at or below 5 wt%. Li et al. [33] investigated dopamine-induced functionalization of CNC with polyethylene glycol (PEG). Lower-molecular weight PEG-functionalized CNCs promoted the crystallization of PLLA with an optimal balance of strength and ductility and also reduced the oxygen permeability coefficient by 66.4% at only 0.5 wt%. Additionally, CNCs grafted with higher-molecular weight PEG chains yield substantial ductility improvements, increasing PLLA elongation by up to 168%. In another study conducted by Pal et al. [34], PLA nanocomposite films reinforced with PEG-grafted TEMPO-oxidized CNCs (PEG-TOCNC) and reduced graphene oxide (rGO) were prepared, achieving improved dispersion and substantial enhancements in mechanical, thermal, and thermomechanical performance.

Although numerous studies have explored the mechanical and thermal enhancements achieved with polymer-grafted CNCs, a comprehensive understanding of the final rheological behavior of such nanocomposites remains limited and requires further investigation. In our recent work, chemical modification of CNCs was implemented through grafting poly(glycidyl methacrylate) (PGMA) with varying chain lengths and the resulting rheological and thermal properties of their nanocomposites with PBAT were examined [35]. Melt rheological and dynamic mechanical analyses revealed that the addition of CNC-*g*-PGMA with longer PGMA molecules in PBAT led to a significant increase in complex viscosity and storage modulus at low frequencies. In this study, using a green, water-based grafting-from method, CNCs were modified with poly(2-hydroxyethyl methacrylate) (PHEMA) using a grafting-from approach to reduce the strong hydrogen bonding responsible for CNC–CNC aggregation, while still introducing hydroxyl-bearing side chains capable of interacting with the polymer matrix. This dual functionality creates a synergistic effect: steric stabilization from the grafted chains suppresses particle–particle interactions and improves dispersion, while the remaining hydroxyl groups on PHEMA promote interfacial adhesion with PBAT through secondary bonding. Because the balance between steric hindrance and interfacial functionality is strongly dependent on graft length, CNCs were functionalized with PHEMA chains of varying lengths to systematically investigate this effect. For comparison, PHEMA homopolymers were also synthesized under identical reaction conditions, enabling a direct evaluation of polymer–matrix interactions in the absence of CNCs. Subsequently, the modified CNCs (mCNCs), neat CNCs, and PHEMA homopolymers were incorporated into PBAT at a given content of 3 wt% via melt mixing.

This design allowed for a comprehensive comparison among PBAT/mCNC, PBAT/neat CNC and PBAT/PHEMA, thereby isolating the individual contributions of CNCs, grafted chains, and homopolymers to the final material behavior. The rheological, thermal, and thermomechanical properties of all systems were thoroughly investigated to clarify the impact of PHEMA chain length and grafting on dispersion and interfacial interactions within PBAT.

2. Experimental

2.1. Materials

Spray-dried CNCs with average length, width, and aspect ratio of, respectively, around 165 nm, 13 nm, and 12.7 were supplied from CelluForce (Montreal, QC, Canada). 2-Hydroxyethyl methacrylate (HEMA, 97%, stabilized) was obtained from Thermo Scientific and subsequently purified by removing the inhibitor through a short alumina (Sigma-Aldrich, Shanghai, China) column. Potassium persulfate (KPS), used as a water-soluble radical initiator, and diethyl ether were supplied from Sigma-Aldrich. Poly(butylene adipate-co-terephthalate) (PBAT, Ecoflex® F Blend C1200) was provided by BASF (Ludwigshafen, Germany).

2.2. Surface Modification of CNC with HEMA (CNC-g-PHEMA)

First, 1 g of CNC was dispersed in 50 mL of distilled water in a round-bottom flask and stirred for 30 min using a magnetic stirrer, followed by 30 min of ultrasonication. Then, 0.1 g of KPS was added and stirred for 5 min before placing the mixture in an oil bath at 70 °C for 5 min. The system was purged with nitrogen, after which varying amounts of HEMA monomer, as noted in Table 1, were added dropwise under continuous stirring. During the grafting reaction, HEMA was introduced slowly into the reaction medium to reduce the likelihood of solution-phase homopolymerization and to promote surface-initiated radical grafting. The reaction was carried out under nitrogen at 70 °C for 3 h. After cooling, the mixture was poured into 250 mL of diethyl ether and stirred for 30 min. The white precipitate was collected and dried. Figure 1 shows the schematic of the noted grafting.

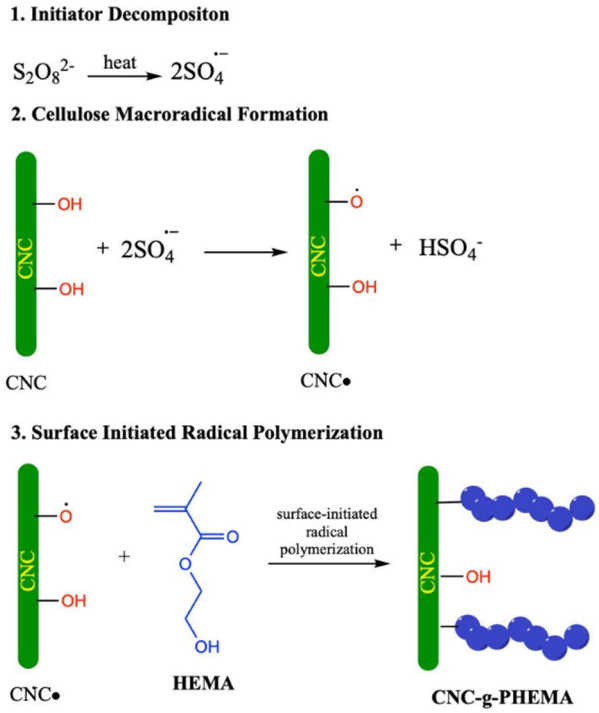


Figure 1. Synthesis of CNC-g-PHEMA (mCNCs).

Table 1. Surface modification of CNCs with different concentrations of HEMA.

Sample Name	Sample Code	CNC Amount (g)	Initiator Amount (g)	HEMA Amount (mL)
CNC-*g*-PHEMA1	mCNC1	1.0	0.1	1
CNC-*g*-PHEMA3	mCNC3	1.0	0.1	3
CNC-*g*-PHEMA5	mCNC5	1.0	0.1	5
CNC-*g*-PHEMA7	mCNC7	1.0	0.1	7
CNC-*g*-PHEMA10	mCNC10	1.0	0.1	10

2.3. Synthesis of PHEMA Homopolymers

KPS (0.1 g) was added to 50 mL of water and stirred for 5 min before placing the mixture in an oil bath at 70 °C for 5 min. The system was purged with nitrogen, after which varying amounts of HEMA monomer (Table 2) were added dropwise under continuous stirring. The reaction was carried out under nitrogen at 70 °C for 3 h. After cooling, PHEMA was precipitated and dried.

Table 2. PHEMA homopolymers with different concentrations of HEMA.

Sample Name	Initiator Amount (g)	HEMA Amount (mL)
PHEMA1	0.1	1
PHEMA3	0.1	3
PHEMA5	0.1	5
PHEMA7	0.1	7
PHEMA10	0.1	10

Comparisons among the PHEMA homopolymers are based on relative variations in monomer feed level and polymerization conditions, rather than on explicitly assigned polymer chain length values.

2.4. Sample Preparation

Modified CNCs and PHEMA samples were melt-mixed with PBAT at a concentration of 3 wt% using an internal melt mixer (Kökbir RTX-M40, Kökbir, Kırklareli, Türkiye) at 160 °C for 5 min with a rotor speed of 100 rpm. Neat CNC was also melt-mixed with PBAT as a reference. Prior to melt-mixing, all materials were dried in a vacuum oven at 50 °C for 6 h. Samples for rheological and thermal analyses were prepared by hot pressing at 160 °C for 5 min under 1.5 bar.

2.5. Fourier Transform Infrared Spectroscopy (FTIR) Analysis

The chemical structures of neat CNC and mCNC samples were characterized by Fourier transform infrared (FTIR) spectroscopy. Spectra were recorded at room temperature over the mid-infrared range (500–4000 cm^{-1}) using a Bruker FTIR spectrometer (Bruker Optik GmbH, Ettlingen, Germany) equipped with a Platinum ATR accessory.

2.6. X-Ray Diffraction (XRD) Analysis

Wide-angle X-ray diffraction (XRD) was employed to assess the crystallinity of CNCs. A copper-anode XRD system (PANalytical B.V., Almelo, The Netherlands) was used to compare neat CNC and mCNC samples, with scans performed over the 10–90° 2θ range.

2.7. Wettability Analysis

The change in hydrophilic behavior of the mCNCs was evaluated by examining neat CNC, mCNCs, and PHEMA5 in a solvent system of water and chloroform, which have different densities (water: ~1.0 g/cm^3; chloroform: ~1.57 g/cm^3). Samples were first placed in water and chloroform was subsequently added.

2.8. Contact Angle Analysis

The hydrophobicity of the surfaces was evaluated by measuring the water contact angle. For this purpose, 150 mg of mCNC powder was compressed at 10 tons for 5 min to obtain smooth-surfaced samples. Water contact angle measurements were performed at multiple locations on each pellet (three measurements per sample) using a KSV CAM 200 goniometer (KSV Instruments, Helsinki, Finland) by placing a 5 µL water droplet on the surface, followed by tangent analysis using ImageJ software (Version 1.54p).

2.9. Thermogravimetric Analysis (TGA)

Thermal stability of neat CNC and mCNCs were analyzed using a METTLER TOLEDO thermogravimetric analyzer (Mettler-Toledo International Inc., Greifensee, Switzerland) under nitrogen, with a heating rate of 10 °C/min up to 800 °C.

2.10. Differential Scanning Calorimetry (DSC) Analysis

The thermal transitions and crystallization behavior of PBAT/CNC, PBAT/mCNC nanocomposites and PBAT/PHEMA compounds were examined using differential scanning calorimetry (DSC, Mettler-Toledo International Inc., Greifensee, Switzerland). Samples were heated from room temperature to 200 °C at 10 °C/min, held at 200 °C for 5 min, cooled to −50 °C at the same rate and subsequently reheated to 200 °C at 10 °C/min. The crystallinity degree of PBAT (X_c) was determined according to Equations (1) and (2).

$$X_c^{heating} = (\Delta H_m) \times 100/w_{PBAT} \times \Delta H_m^0 \quad (1)$$

$$X_c^{cooling} = (\Delta H_C) \times 100/w_{PBAT} \times \Delta H_m^0 \quad (2)$$

Here, W_{PBAT} represents the weight fraction of PBAT, while ΔH_m and ΔH_c correspond to the enthalpies of melting and crystallization, respectively. ΔH_m^0 is the enthalpy of fusion for 100% crystalline PBAT, reported as 114 J/g [36].

2.11. Melt Rheological Analysis

Small-amplitude oscillatory shear melt rheological experiments were performed to evaluate the dispersion of mCNCs within the polymer matrix and the interfacial interactions between the matrix and mCNCs. Measurements were carried out under nitrogen using an MCR302 rotational rheometer (Anton Paar, Graz, Austria) with a 25 mm parallel-plate geometry and a 1 mm gap. Frequency sweep tests were conducted at 160 °C with 1% strain.

2.12. Dynamic Mechanical Analysis (DMA)

The thermomechanical properties of PBAT/mCNC nanocomposites and PBAT/PHEMA compounds were investigated using a dynamic mechanical analyzer (DMA Anton Paar MCR302e, Anton Paar GmbH, Graz, Austria). Rectangular specimens (35 × 10 × 2 mm) were tested in single cantilever mode and heated from room temperature to 120 °C at 3 °C/min, with a deformation amplitude of 30 µm and a frequency of 1 Hz.

3. Results and Discussion

3.1. Characterization of mCNCs and PHEMAs

Throughout this study, surface modification levels are discussed in a relative and comparative manner, based on monomer feed concentration and the resulting structure–property trends, rather than on quantitatively determined graft density or polymer chain length.

Following the grafting reaction, the modified CNCs were subjected to repeated washing and centrifugation steps to remove unreacted monomer and soluble polymer species. To further reduce the formation of free PHEMA homopolymers during the grafting process, the HEMA monomer was introduced slowly and in a controlled manner into the reaction medium. Gradual monomer addition is known to suppress solution-phase homopolymerization by favoring surface-initiated radical reactions over bulk polymerization. Although these measures significantly reduce the likelihood of extensive homopolymer formation, the possible presence of small amounts of physically associated PHEMA chains on the CNC surface cannot be completely excluded.

FTIR spectroscopy was employed to evaluate the surface modification of CNCs with PHEMA (Figure 2). Relative to neat CNC, the CNC-*g*-PHEMA samples exhibited a distinct absorption band around 1720 cm^{-1}, corresponding to the C=O stretching of ester groups, confirming successful grafting of PHEMA onto the CNC surface. Moreover, a pronounced increase in absorbance within the 1140–1190 cm^{-1} region, associated with C–O stretching vibrations of ester groups, provided additional evidence of graft formation. The broad O–H stretching band near 3340 cm^{-1}, typical of the hydroxyl-rich CNC structure, was still present after modification due to hydroxyl groups of both CNC and PHEMA, although slight changes in intensity and band shape were observed. Furthermore, the characteristic glycosidic C–O–C band at 1050–1030 cm^{-1} confirmed retention of the cellulose backbone, with fluctuations at higher grafting levels. While FTIR spectroscopy confirms the presence of PHEMA-related functional groups on the CNC surface, it does not allow unambiguous identification of the exact bonding nature (covalent grafting versus strong hydrogen bonding). Accordingly, the proposed modification mechanism is inferred from the reaction conditions and is consistent with well-established potassium persulfate-initiated radical grafting-from processes.

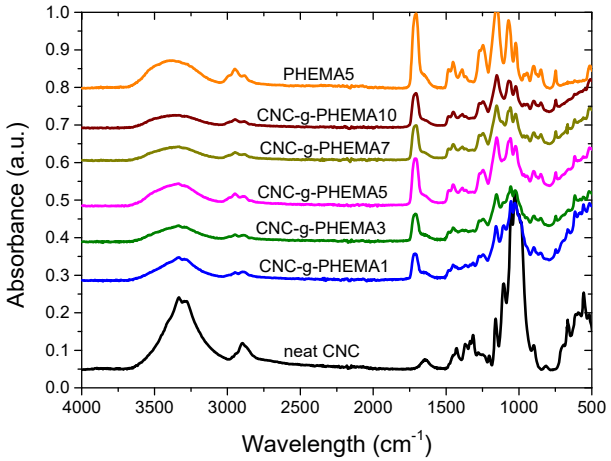


Figure 2. FTIR spectra of neat CNC, mCNCs and PHEMA5.

To evaluate the effect of PHEMA grafting on the crystalline structure of CNC, XRD analysis was performed on neat CNC, CNC-*g*-PHEMA samples with varying grafting ratios, and pure PHEMA (Figure 3). The diffractogram of neat CNC exhibits three characteristic reflections at approximately $2\theta \approx 16$, 23, and 34, which can be assigned to the (110), (200),

and (004) crystallographic planes of cellulose, respectively. These peaks are consistent with the typical diffraction pattern reported for nanocrystalline cellulose in the literature [37–39]. In contrast, the diffraction pattern of pure PHEMA displays predominantly broad and diffuse peaks, confirming its largely amorphous nature. A broad maximum is observed at approximately 19.5°, accompanied by additional features centered around 30° and 42° [40,41]. The absence of sharp reflections indicates the lack of long-range crystalline order in PHEMA. Upon grafting PHEMA onto CNC, the characteristic cellulose reflections remain detectable, indicating that the crystalline structure of CNC is largely preserved after surface modification. However, a progressive reduction in peak intensity and slight broadening of the cellulose reflections are observed with increasing PHEMA content. This behavior can be attributed to (i) the increasing amorphous contribution from grafted PHEMA chains [35], (ii) partial attenuation of CNC scattering due to surface coverage [42,43] and (iii) possible slight reductions in coherent crystallite size or crystallinity [44]. Additionally, minor diffuse features are occasionally detected in the 28–32° and 40–45° regions for neat CNC and CNC-g-PHEMA samples. Their diffuse nature suggests that they originate from short-range structural ordering within amorphous domains, particularly from the grafted PHEMA matrix, rather than from secondary crystalline impurities.

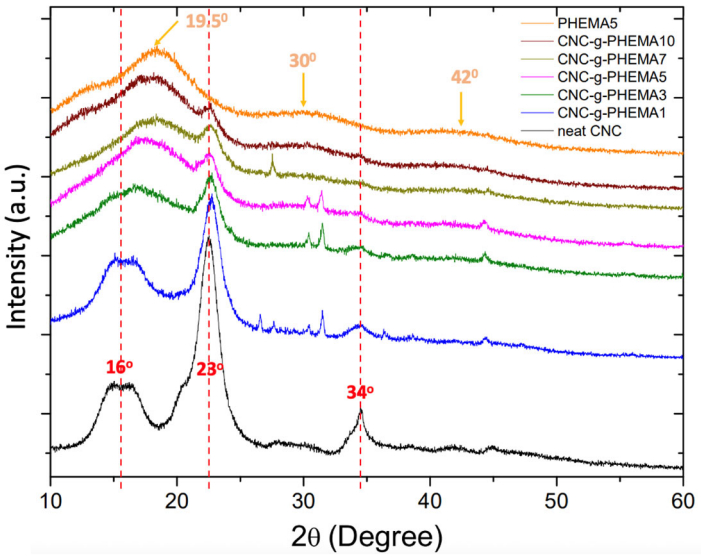


Figure 3. X-ray diffraction patterns of neat CNC, mCNCs and PHEMA5.

Figure 4 shows that neat CNCs exhibit a water contact angle of 42°. Increasing the amount of HEMA used during grafting (1, 3, and 5 mL) raised the contact angle to 51°, 61°, and 68°, respectively, indicating that substitution of surface hydroxyl groups with PHEMA chains reduces surface polarity and increases hydrophobicity. However, when the HEMA amount was further increased to 7 and 10 mL, the contact angle sharply decreased to 27° and 30°. This reversal can be attributed to two mechanistic effects supported by the literature: (i) longer PHEMA chains tend to adopt coiled or looped conformations in the dry state, causing the outermost surface to be enriched in hydrophilic groups (pendant –OH groups). A similar trend was reported by Yoshikawa et al., [45] who observed that longer PHEMA brush chains produced slightly lower water contact angles than shorter ones, indicating that increased chain length can enrich the surface with hydrophilic segments and thereby enhance wettability. (ii) Elevated monomer concentrations also promote competitive homopolymerization by nature, generating PHEMA chains that may adsorb onto CNC surfaces or become entrapped within the grafted layer, thereby increasing the exposure of polar groups. Although PHEMA is intrinsically hydrophilic, covalent grafting of PHEMA onto CNCs at moderate grafting density reduces the apparent hydrophilicity by partially

masking the highly ordered and densely packed hydroxyl groups on the crystalline CNC surface. In neat CNCs, these regularly arranged –OH groups are rigid, closely spaced, and highly accessible, resulting in strong hydrogen bonding with water [46]. When PHEMA chains are chemically bound to the surface, they have restricted mobility, and hence, they form a constrained polymer layer that disrupts direct water access to the crystalline cellulose lattice and lowers the effective surface energy, despite the presence of hydrophilic functionalities within the grafted chains. In contrast, at high monomer concentrations, the formation of PHEMA homopolymers introduces mobile, non-tethered chains that can adsorb onto the CNC surface or dominate the outermost interface. These freely mobile chains readily expose their hydroxyl groups to water and can adopt hydrated coil conformations, thereby increasing the density and accessibility of polar groups at the surface and restoring—or even enhancing—the hydrophilic character. Similar effects of random-coil polymer conformation on surface wettability have been reported, where mobile polymer chains reorganize at interfaces and dominate surface energy despite chemical composition [42]. To suppress homopolymer formation to some extent, the HEMA monomer was added slowly to favor surface-initiated grafting in all samples; however, at higher monomer concentrations, some homopolymerization is likely unavoidable. Under these conditions, CNC-*g*-PHEMA5 exhibited the highest hydrophobicity among all samples.

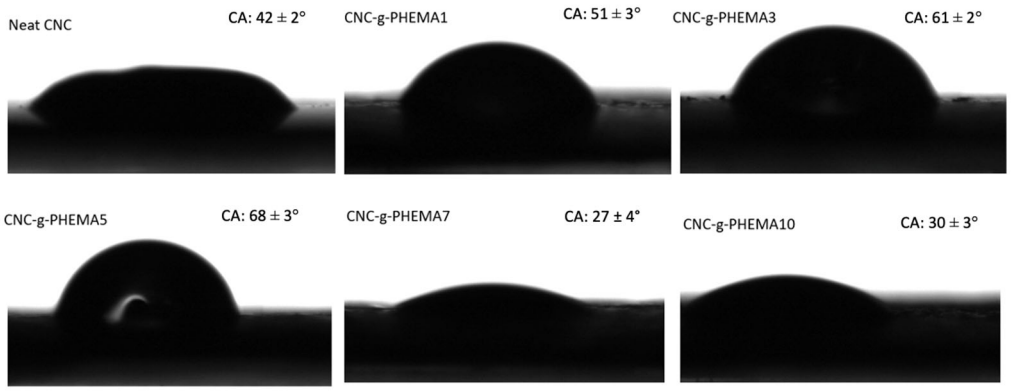


Figure 4. Water contact angles of neat CNC and mCNCs.

The change in the surface hydrophilicity of CNCs was further qualitatively supported by the wettability test. In this test, the samples were first dispersed in water, followed by the addition of chloroform to form a biphasic system (Figure 5). As shown in Figure 5a, neat CNC remained fully dispersed in the water, confirming its strongly hydrophilic character. In contrast, all PHEMA-grafted CNC samples gradually settled toward the bottom of the vial, indicating a reduction in surface hydrophilicity following grafting. Upon addition of chloroform (Figure 5b), distinct differences in phase preference became evident. Among the modified samples, CNC-*g*-PHEMA5 (mCNC5) exhibited the most pronounced migration toward the chloroform phase, demonstrating the highest affinity for the organic solvent and thus the greatest surface hydrophobicity. Samples with lower or higher grafting levels showed weaker partitioning into the chloroform phase. After 30 min of settling (Figure 5c), the phase distributions remained largely unchanged, indicating that the observed partitioning behavior is stable and governed by intrinsic surface wettability.

Figure 6 shows the TGA curves of neat CNC, PHEMA-grafted CNCs (mCNCs), and PHEMA homopolymers. A small initial mass loss below approximately 100 °C is observed for all samples. This weight loss is attributed to the evaporation of physically adsorbed moisture. CNC contains abundant surface hydroxyl groups that readily retain atmospheric water, while PHEMA may also contain residual solvent or bound moisture. Therefore, this low-temperature mass loss is consistent with the hygroscopic nature of both compo-

nents. As shown in Figure 6a, neat CNC exhibits a single major degradation step cantered around 300 °C, characteristic of cellulose thermal decomposition. This process involves depolymerization, dehydration, and subsequent aromatization reactions, which lead to the formation of carbonaceous char residue at elevated temperatures. Neat CNC exhibits a relatively high char yield due to cellulose dehydration and carbonaceous residue formation during pyrolysis [47]. Pure PHEMA (Figure 6b), in contrast, undergoes major degradation between approximately 300 and 420 °C and leaves only a small residual mass, confirming that PHEMA predominantly decomposes through depolymerization and volatilization with minimal char formation [48]. Interestingly, CNC-*g*-PHEMA1 shows a slightly higher residue than neat CNC. At low grafting density, interfacial interactions between CNC and surface-bound PHEMA chains may promote localized stabilization and enhanced carbonaceous structure formation during pyrolysis, leading to a mild synergistic increase in char yield. Similar effects have been reported for chemically modified cellulose systems, where surface esterification or small-molecule grafting altered the pyrolysis pathway and slightly enhanced char formation [49]. Therefore, at low grafting density, interfacial interactions between CNC and surface-bound PHEMA chains may influence localized carbonization behavior. However, as the PHEMA grafting ratio increases (CNC-*g*-PHEMA3 to CNC-*g*-PHEMA10), the overall residue decreases significantly. This trend is consistent with the increasing fraction of PHEMA, which produces minimal char. Notably, the thermal profiles of CNC-*g*-PHEMA7 and CNC-*g*-PHEMA10 closely resemble that of the PHEMA5 homopolymer, suggesting that the CNC surface is increasingly dominated by PHEMA, either through extensive chain grafting, chain coiling, or the presence of PHEMA homopolymers. This observation is consistent with the contact angle results, which indicate a PHEMA-rich surface at higher grafting levels.



Figure 5. Wettability test of neat CNC, mCNCs and PHEMA5 in (**a**) water, (**b**) water with chloroform at t = 0, and (**c**) water with chloroform after 30 min (t = 30 min).

Figure 6b presents the TGA curves of the PHEMA homopolymers, all of which display two-step degradation between approximately 250 °C and 400 °C. PHEMA1, containing the shortest polymer chains, degrades at the lowest temperatures. Increasing monomer concentration improves thermal stability up to PHEMA3 and PHEMA5, while PHEMA7 and PHEMA10 show earlier degradation, likely due to the formation of a higher frac-

tion of shorter or defect-rich chains during radical polymerization at elevated monomer concentrations.

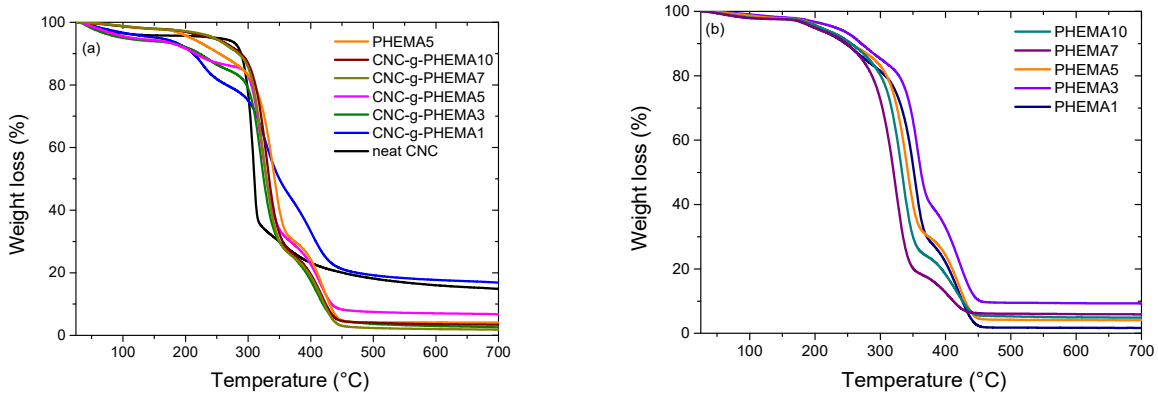


Figure 6. TGA curve of (**a**) neat CNC, mCNCs and PHEMA5 and (**b**) PHEMA homopolymers.

3.2. Characterization of PBAT-Based Nanocomposites and Compounds

DSC analysis of neat PBAT, PBAT/CNC, PBAT/mCNC nanocomposites, and PBAT/PHEMA compounds (Figure 7 and Table 3) shows that neat PBAT exhibits the lowest crystallization temperature (T_c = 67.56 °C). The incorporation of neat CNC increases T_c to 73.87 °C, indicating a heterogeneous nucleation effect. For PBAT/mCNC nanocomposites and PBAT/PHEMA compounds, T_c values span a wider range (≈71–84 °C), reflecting the combined influence of CNC surface chemistry and polymer chain mobility on crystallization onset.

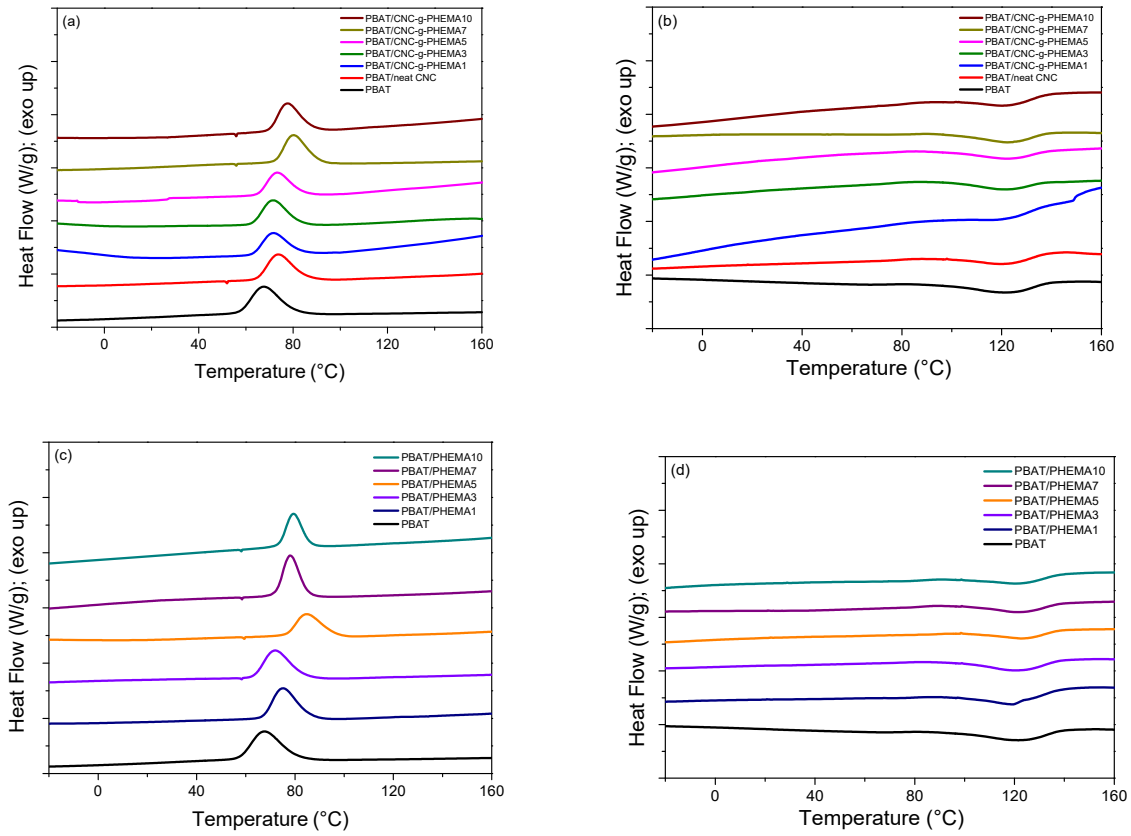


Figure 7. Cooling (**a**,**c**) and second heating (**b**,**d**) DSC curves of PBAT, PBAT/neat CNC and PBAT/mCNC nanocomposites (**a**,**b**) and PBAT and PBAT/PHEMA compounds (**c**,**d**).

Table 3. DSC results of neat PBAT, PBAT/neat CNC, PBAT/mCNC nanocomposites and PBAT/PHEMA compounds for cooling and second heating scans.

Samples	Crystallization and Melting Temperatures		Degree of Crystallinity (%)	
	T_c	T_m	X_c	X_m
Neat PBAT	67.6	122.0	21.4	13.3
PBAT/neat CNC	73.9	121.5	17.3	10.9
PBAT/CNC-*g*-PHEMA1	71.7	122.8	14.2	28.0
PBAT/CNC-*g*-PHEMA3	71.5	121.4	16.1	8.7
PBAT/CNC-*g*-PHEMA5	73.2	122.6	14.1	9.9
PBAT/CNC-*g*-PHEMA7	80.2	122.8	16.8	11.0
PBAT/CNC-*g*-PHEMA10	77.5	121.9	16.4	9.8
PBAT/PHEMA1	75.2	119.5	18.6	15.0
PBAT/PHEMA3	72.0	121.1	17.4	13.1
PBAT/PHEMA5	84.7	123.5	14.4	7.8
PBAT/PHEMA7	78.1	122.3	16.8	9.8
PBAT/PHEMA10	79.2	121.5	13.5	9.6

Despite the increase in T_c, the degree of crystallinity calculated from the cooling scans (X_c) generally decreases upon CNC addition and remains comparable to that of neat PBAT in CNC-*g*-PHEMA nanocomposites, suggesting that while crystallization is initiated earlier, the overall extent of crystal formation during cooling is restricted. This behavior is attributed to constrained PBAT chain mobility within the filler–polymer interphase.

Notably, PBAT/CNC-*g*-PHEMA7 and PBAT/CNC-*g*-PHEMA10 exhibit higher and sharper crystallization peaks, indicating faster crystallization kinetics. A similar trend is observed for PBAT/PHEMA7 and PBAT/PHEMA10, which display narrower and more intense crystallization peaks. This behavior suggests accelerated crystallization, likely associated with the presence of shorter PHEMA homopolymer chains that can reorganize more readily, in agreement with the earlier degradation behavior observed in the TGA results of the corresponding PHEMA homopolymers.

The degree of crystallinity calculated from the second heating scans (X_m) varies among the samples, with most CNC-*g*-PHEMA nanocomposites exhibiting values comparable to or slightly lower than neat PBAT. Across all formulations, the melting temperature (T_m) remains relatively constant in the range of 119–123 °C, indicating that the crystalline structure of PBAT is largely preserved despite the presence of CNCs or PHEMA.

Rheological analysis (Figure 8a,b) shows that PBAT/CNC-*g*-PHEMA5 exhibits the highest complex viscosity (η*) and storage modulus (G′) in the low-frequency region, indicating the formation of a more developed filler–polymer network within the PBAT matrix. At this optimal grafting level, PHEMA chains of suitable length are grown from the CNC surface, which effectively suppresses CNC–CNC hydrogen bonding while promoting interfacial interactions with PBAT.

In contrast, PBAT/CNC-g-PHEMA1 and PBAT/CNC-g-PHEMA3 display lower viscosity and modulus values, particularly at low frequencies. The shorter grafted chains in these systems are insufficient to fully disrupt the strong intermolecular hydrogen bonding between CNC particles, leading to limited dispersion within the PBAT matrix. As a result, network formation is less effective and the rheological enhancement remains limited.

For PBAT/CNC-*g*-PHEMA7 and PBAT/CNC-*g*-PHEMA10, the rheological response again diminishes relative to CNC-*g*-PHEMA5. At higher HEMA contents, excessive grafting likely results in long PHEMA chains that coil or collapse on the CNC surface, over-covering the nanofiller and hindering CNC–CNC and CNC–PBAT interactions necessary for network formation [50,51]. In addition, elevated monomer concentrations during grafting may

promote competitive homopolymerization, generating PHEMA homopolymers that adsorb onto CNC surfaces and further limit effective dispersion.

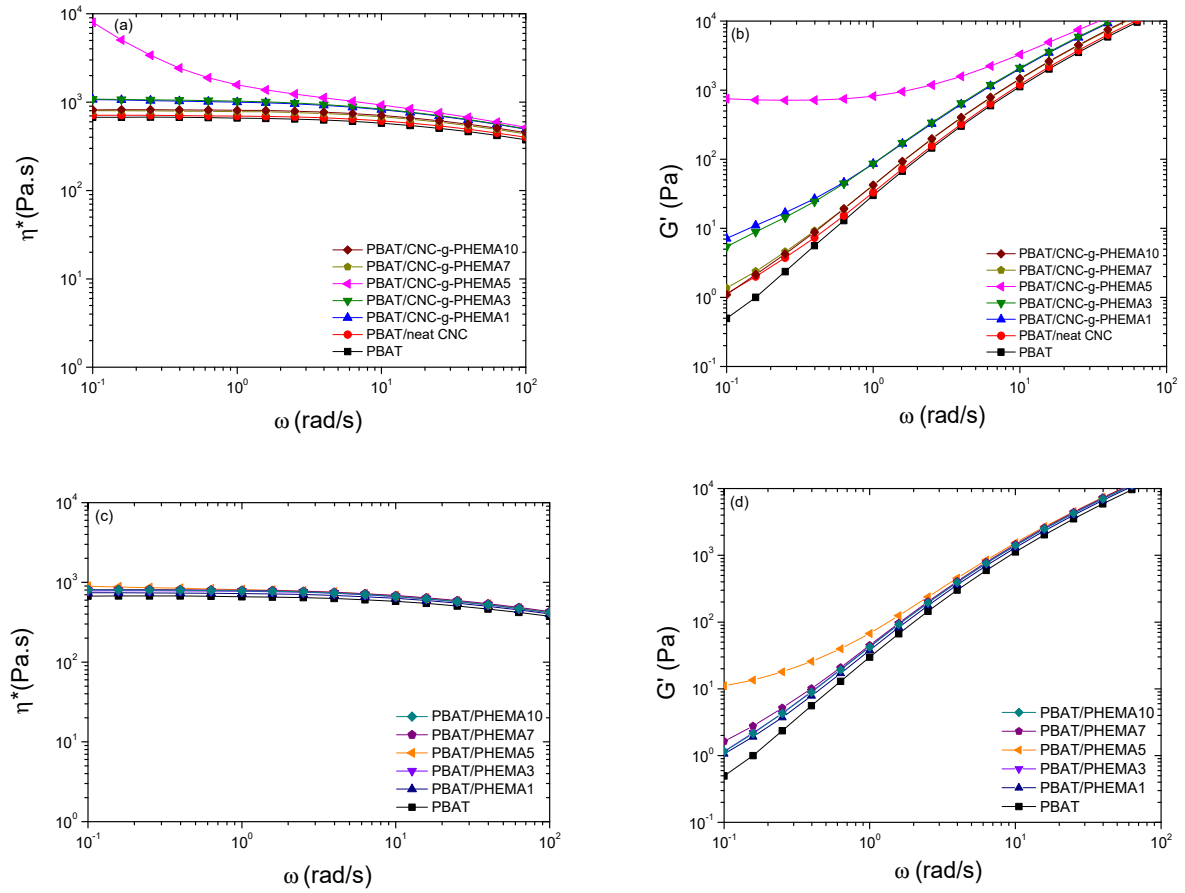


Figure 8. Complex viscosity (**a**,**c**) and storage modulus (**b**,**d**) of PBAT, PBAT/neat CNC and PBAT/mCNC nanocomposites (**a**,**b**) and PBAT and PBAT/PHEMA compounds (**c**,**d**) measured at 160 °C.

Figure 8c,d show that among the PBAT/PHEMA compounds, PBAT/PHEMA5 exhibits the highest complex viscosity and storage modulus. However, the magnitude of rheological enhancement in PBAT/CNC-*g*-PHEMA5 is significantly greater than that observed in PBAT/PHEMA systems, highlighting the synergistic role of well-dispersed, surface-modified CNCs in reinforcing the PBAT matrix through combined filler networking and interfacial interactions.

A comparison with our previously reported CNC-*g*-PGMA/PBAT nanocomposites reveals consistent trends as well as notable differences arising from side-chain chemistry [27]. In both systems, surface-modified CNCs induce pronounced increases in low-frequency complex viscosity and storage modulus relative to neat PBAT, with the strongest rheological enhancement observed at intermediate modification levels. This behavior is indicative of reduced CNC agglomeration during melt processing. Compared to CNC-*g*-PGMA, CNC-*g*-PHEMA nanocomposites exhibit a more pronounced increase in low-frequency storage modulus and complex viscosity, suggesting the formation of a stronger rheological network. This difference can be attributed to the hydroxyl-rich PHEMA side chains, which enable enhanced hydrogen-bond-mediated interactions between CNCs as well as between CNCs and the PBAT matrix. In contrast, PGMA-grafted CNCs primarily promote compatibilization and dispersion with a comparatively weaker contribution to long-time elastic response.

It should be noted that the observed low-frequency increases in storage modulus and complex viscosity may arise from multiple contributing mechanisms. In addition to interaction-driven network formation, factors such as hydrodynamic effects, local phase thickening, and the possible presence of residual or physically associated PHEMA chains may also influence the viscoelastic response [52]. Nevertheless, the systematic evolution of rheological behavior across the sample series suggests that enhanced CNC dispersion, arising from strengthened filler–matrix interactions, represents the dominant contribution to the observed rheological enhancement.

Figure 9 presents the temperature dependence of the storage modulus (E′) and tan δ of PBAT/mCNC nanocomposites and PBAT/PHEMA compounds. All samples exhibit a gradual decrease in E′ beginning around 45 °C (Figure 9a,b), which is attributed to the onset of molecular mobility associated with the terephthalate segments of PBAT [53]. The absence of sudden modulus drops indicates that the thermomechanical stability of PBAT is preserved upon incorporation of CNCs or PHEMA. The tan δ curves (Figure 9c,d) display minimal variation among all samples, with no pronounced shift in peak position or intensity. This indicates that neither CNC grafting nor PHEMA incorporation substantially affects the glass transition behavior or damping characteristics of PBAT, suggesting good interfacial compatibility and the absence of phase separation. Overall, DMA results confirm that the enhanced viscoelastic behavior observed in melt rheology arises primarily from filler network formation in the molten state, while the solid-state thermomechanical properties of PBAT remain largely unchanged.

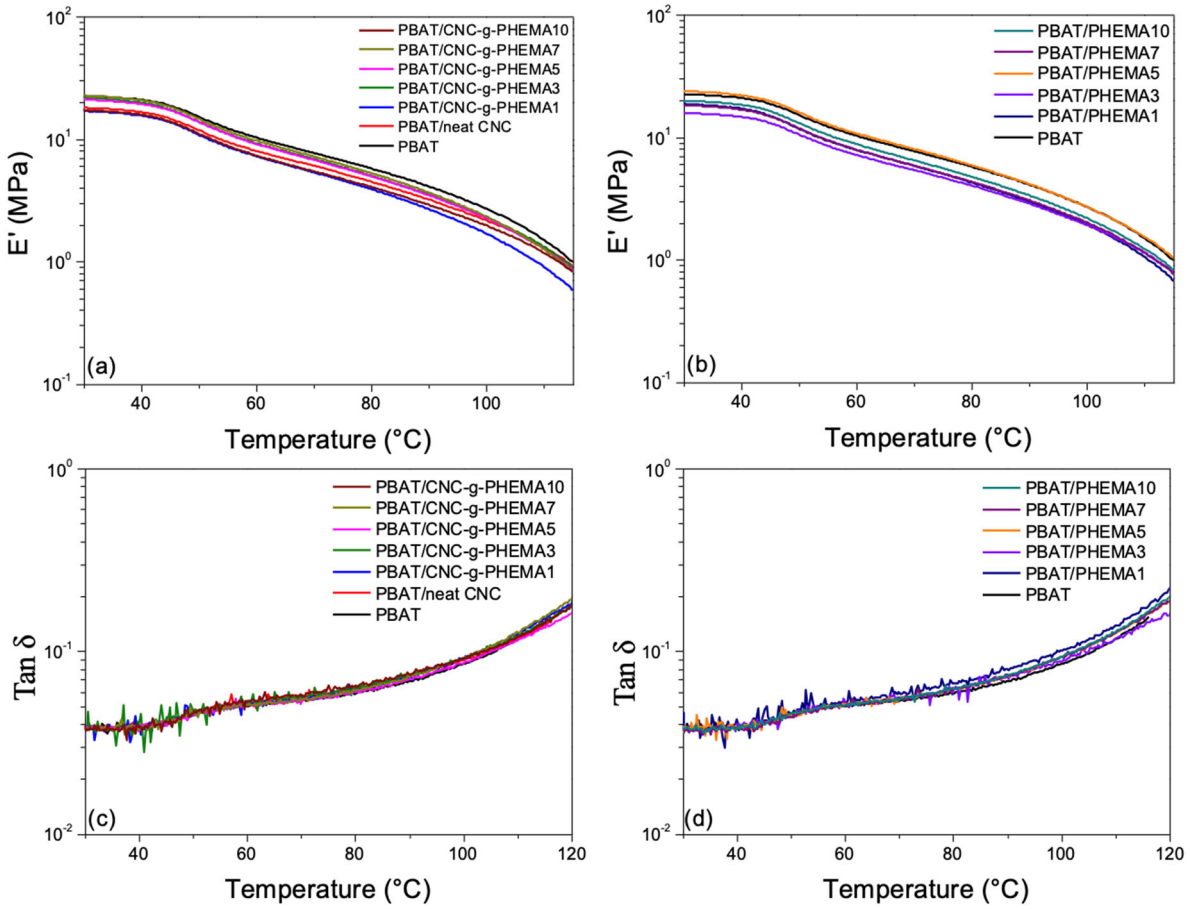


Figure 9. Temperature dependence of the storage modulus (**a**,**b**) and tan δ curves (**c**,**d**) of PBAT, PBAT/neat CNC and PBAT/mCNC nanocomposites (**a**,**c**) and PBAT and PBAT/PHEMA compounds (**b**,**d**).

4. Conclusions

This study systematically investigated the surface modification of CNC with poly(2-hydroxyethyl methacrylate) (PHEMA) via a grafting-from approach to mitigate strong CNC–CNC intermolecular hydrogen bonding and to enhance interfacial interactions with a PBAT matrix. By tailoring the PHEMA grafting degree, the influence of polymer chain length on CNC dispersion, surface wettability, and melt-state behavior was explained. The results demonstrate that controlled surface modification effectively balances the reduction in CNC hydrophilicity while preserving favorable interactions with the polymer matrix through accessible hydroxyl functionalities.

Contact angle and wettability tests consistently revealed that CNC-*g*-PHEMA5 exhibits the highest hydrophobicity. Rheological analysis further confirmed that the PBAT/CNC-g-PHEMA5 nanocomposite displays the highest complex viscosity and storage modulus at low frequencies, evidencing the formation of an effective filler–polymer network. This enhanced viscoelastic response is attributed to the presence of PHEMA chains of appropriate length, which suppress CNC aggregation, promote developed dispersion, and facilitate interfacial interactions with PBAT.

Overall, CNC-*g*-PHEMA5, representing an intermediate grafting level, provides an optimal balance between surface hydrophobicity, interfacial compatibility, and network formation, resulting in superior dispersion and rheological performance within the PBAT matrix. These findings highlight the critical role of controlled polymer grafting in designing CNC-based nanocomposites and offer a viable strategy for developing well-dispersed, high-performance, and sustainably processed biopolymer composites suitable for melt-processing applications.

Future work will also focus on comprehensive mechanical characterization, including tensile, flexural, and impact testing, to further assess the suitability of CNC-*g*-PHEMA-modified PBAT composites for practical applications.

Author Contributions: E.J.Y.A.: conceptualization, investigation, methodology, data curation, visualization, writing—original draft. Y.A.G.: conceptualization, investigation, methodology, visualization, writing—original draft. A.A.: investigation, data curation. E.V.: investigation, data curation. S.E.A.: investigation, data curation. Y.Z.B.: investigation, visualization. M.N.: conceptualization, methodology, validation, writing—review and editing, supervision. All authors have read and agreed to the published version of the manuscript.

Funding: This research was funded by [Istanbul Technical University Research Fund (ITU BAP—YAP)] grant number [43944].

Data Availability Statement: The data presented in this study are available on request from the corresponding author.

Acknowledgments: The authors would like to acknowledge financial support from the Istanbul Technical University Scientific Research Project (ITU-BAP, YAP) with the project number 43944.

Conflicts of Interest: The authors declare no conflicts of interest.

References

1. Jiao, J.; Zeng, X.; Huang, X. An overview on synthesis, properties and applications of poly(butylene-adipate-co-terephthalate)–PBAT. *Adv. Ind. Eng. Polym. Res.* **2020**, *3*, 19–26. [CrossRef]
2. Habibi, Y. Key advances in the chemical modification of nanocelluloses. *Chem. Soc. Rev.* **2014**, *43*, 1519–1542. [CrossRef]
3. Aziz, T.; Ullah, A.; Zeb, U.; Hussain, M.; Ali, A.; Haq, F.; Kiran, M. Advancements in cellulose nanocrystals: A review of functionalization, applications, and challenges. *Int. J. Biol. Macromol.* **2025**, *315*, 144552. [CrossRef]
4. Ghasemlou, M.; Daver, F.; Ivanova, E.P.; Habibi, Y.; Adhikari, B. Surface modifications of nanocellulose: From synthesis to high-performance nanocomposites. *Prog. Polym. Sci.* **2021**, *119*, 101418. [CrossRef]

5. Ferreira, F.V.; Dufresne, A.; Pinheiro, I.F.; Souza, D.H.S.; Gouveia, R.F.; Mei, L.H.I.; Lona, L.M.F. How do cellulose nanocrystals affect the overall properties of biodegradable polymer nanocomposites: A comprehensive review. *Eur. Polym. J.* **2018**, *108*, 274–285. [CrossRef]
6. Mokhena, T.C.; Sadiku, E.R.; Mochane, M.J.; Ray, S.S.; John, M.J.; Mtibe, A. Mechanical properties of cellulose nanofibril papers and their bionanocomposites: A review. *Carbohydr. Polym.* **2021**, *273*, 118507. [CrossRef] [PubMed]
7. Babaei-Ghazvini, A.; Vafakish, B.; Patel, R.; Falua, K.J.; Dunlop, M.J.; Acharya, B. Cellulose nanocrystals in the development of biodegradable materials: A review on CNC resources, modification, and their hybridization. *Int. J. Biol. Macromol.* **2024**, *258*, 128834. [CrossRef] [PubMed]
8. Habibi, Y.; Lucia, L.A.; Rojas, O.J. Cellulose Nanocrystals: Chemistry, Self-Assembly, and Applications. *Chem. Rev.* **2010**, *110*, 3479–3500. [CrossRef] [PubMed]
9. Nagalakshmaiah, M.; Rajinipriya, M.; Afrin, S.; Ansari, M.A.; Asad, M.; Karim, Z. Cellulose Nanocrystals-Based Nanocomposites. In *Bio-Based Polymers and Nanocomposites*; Springer International Publishing: Cham, Switzerland, 2019; pp. 49–65. [CrossRef]
10. Moon, R.J.; Martini, A.; Nairn, J.; Simonsen, J.; Youngblood, J. Cellulose nanomaterials review: Structure, properties and nanocomposites. *Chem. Soc. Rev.* **2011**, *40*, 3941. [CrossRef]
11. Jonoobi, M.; Oladi, R.; Davoudpour, Y.; Oksman, K.; Dufresne, A.; Hamzeh, Y.; Davoodi, R. Different preparation methods and properties of nanostructured cellulose from various natural resources and residues: A review. *Cellulose* **2015**, *22*, 935–969. [CrossRef]
12. Azizi Samir, M.A.S.; Alloin, F.; Sanchez, J.-Y.; El Kissi, N.; Dufresne, A. Preparation of Cellulose Whiskers Reinforced Nanocomposites from an Organic Medium Suspension. *Macromolecules* **2004**, *37*, 1386–1393. [CrossRef]
13. Azeredo, H.M.C.; Rosa, M.F.; Mattoso, L.H.C. Nanocellulose in bio-based food packaging applications. *Ind. Crops Prod.* **2017**, *97*, 664–671. [CrossRef]
14. Vatansever, E.; Arslan, D.; Nofar, M. Polylactide cellulose-based nanocomposites. *Int. J. Biol. Macromol.* **2019**, *137*, 912–938. [CrossRef]
15. Ryoo, J.; Oh, D.X.; Park, J. Engineering Poly(Lactic Acid)/Cellulose Nanocrystal Composites: A Comparative Review of Preparation Strategies and their Influence on Structure-Property Relationships. *Adv. Sustain. Syst.* **2025**, *9*, e00654. [CrossRef]
16. Arslan, D.; Vatansever, E.; Sarul, D.S.; Kahraman, Y.; Gunes, G.; Durmus, A.; Nofar, M. Effect of preparation method on the properties of polylactide/cellulose nanocrystal nanocomposites. *Polym. Compos.* **2020**, *41*, 4170–4180. [CrossRef]
17. Vatansever, E.; Arslan, D.; Sarul, D.S.; Kahraman, Y.; Nofar, M. Effects of molecular weight and crystallizability of polylactide on the cellulose nanocrystal dispersion quality in their nanocomposites. *Int. J. Biol. Macromol.* **2020**, *154*, 276–290. [CrossRef]
18. Sarul, D.S.; Arslan, D.; Vatansever, E.; Kahraman, Y.; Durmus, A.; Salehiyan, R.; Nofar, M. Preparation and characterization of PLA/PBAT/CNC blend nanocomposites. *Colloid Polym. Sci.* **2021**, *299*, 987–998. [CrossRef]
19. Mohammadi, M.; Bruel, C.; Heuzey, M.-C.; Carreau, P.J. CNC dispersion in PLA and PBAT using two solvents: Morphological and rheological properties. *Cellulose* **2020**, *27*, 9877–9892. [CrossRef]
20. Rhim, J.; Mohanty, A.K.; Singh, S.P.; Ng, P.K.W. Effect of the processing methods on the performance of polylactide films: Thermocompression versus solvent casting. *J. Appl. Polym. Sci.* **2006**, *101*, 3736–3742. [CrossRef]
21. Özdemir, B.; Nofar, M. Effect of solvent type on the dispersion quality of spray-and freeze-dried CNCs in PLA through rheological analysis. *Carbohydr. Polym.* **2021**, *268*, 118243. [CrossRef] [PubMed]
22. Sarul, D.S.; Arslan, D.; Vatansever, E.; Kahraman, Y.; Durmus, A.; Salehiyan, R.; Nofar, M. Effect of Mixing Strategy on the Structure-Properties of the PLA/PBAT Blends Incorporated with CNC. *J. Renew. Mater.* **2022**, *10*, 149–164. [CrossRef]
23. Kargarzadeh, H.; Mariano, M.; Huang, J.; Lin, N.; Ahmad, I.; Dufresne, A.; Thomas, S. Recent developments on nanocellulose reinforced polymer nanocomposites: A review. *Polymer* **2017**, *132*, 368–393. [CrossRef]
24. Bagheriasl, D.; Safdari, F.; Carreau, P.J.; Dubois, C.; Riedl, B. Development of cellulose nanocrystal-reinforced polylactide: A comparative study on different preparation methods. *Polym. Compos.* **2019**, *40*, E342–E349. [CrossRef]
25. Mariano, M.; El Kissi, N.; Dufresne, A. Cellulose nanocrystals and related nanocomposites: Review of some properties and challenges. *J. Polym. Sci. B Polym. Phys.* **2014**, *52*, 791–806. [CrossRef]
26. Dufresne, A. Nanocellulose: A new ageless bionanomaterial. *Mater. Today* **2013**, *16*, 220–227. [CrossRef]
27. Bangar, S.P.; Harussani, M.M.; Ilyas, R.A.; Ashogbon, A.O.; Singh, A.; Trif, M.; Jafari, S.M. Surface modifications of cellulose nanocrystals: Processes, properties, and applications. *Food Hydrocoll.* **2022**, *130*, 107689. [CrossRef]
28. Miao, C.; Hamad, W.Y. Cellulose reinforced polymer composites and nanocomposites: A critical review. *Cellulose* **2013**, *20*, 2221–2262. [CrossRef]
29. Trache, D.; Tarchoun, A.F.; Derradji, M.; Hamidon, T.S.; Masruchin, N.; Brosse, N.; Hussin, M.H. Nanocellulose: From Fundamentals to Advanced Applications. *Front. Chem.* **2020**, *8*, 392. [CrossRef]
30. Zhang, X.; Zhang, Y. Reinforcement effect of poly(butylene succinate) (PBS)-grafted cellulose nanocrystal on toughened PBS/polylactic acid blends. *Carbohydr. Polym.* **2016**, *140*, 374–382. [CrossRef]

31. Rosli, N.A.; Ahmad, I.; Anuar, F.H.; Abdullah, I. Application of polymethylmethacrylate-grafted cellulose as reinforcement for compatibilised polylactic acid/natural rubber blends. *Carbohydr. Polym.* **2019**, *213*, 50–58. [CrossRef] [PubMed]
32. Spinella, S.; Samuel, C.; Raquez, J.-M.; McCallum, S.A.; Gross, R.; Dubois, P. Green and Efficient Synthesis of Dispersible Cellulose Nanocrystals in Biobased Polyesters for Engineering Applications. *ACS Sustain. Chem. Eng.* **2016**, *4*, 2517–2527. [CrossRef]
33. Li, L.; Bao, R.Y.; Gao, T.; Liu, Z.Y.; Xie, B.H.; Yang, M.B.; Yang, W. Dopamine-induced functionalization of cellulose nanocrystals with polyethylene glycol towards poly(L-lactic acid) bionanocomposites for green packaging. *Carbohydr. Polym.* **2019**, *203*, 275–284. [CrossRef]
34. Pal, N.; Banerjee, S.; Roy, P.; Pal, K. Reduced graphene oxide and PEG-grafted TEMPO-oxidized cellulose nanocrystal reinforced poly-lactic acid nanocomposite film for biomedical application. *Mater. Sci. Eng. C* **2019**, *104*, 109956. [CrossRef]
35. Arslan, O.N.; Güntürkün, D.; Göksu, Y.A.; Altınbay, A.; Özer, H.Ö.; Nofar, M. Poly(glycidyl methacrylate) modified cellulose nanocrystals and their PBAT-based nanocomposites. *Int. J. Biol. Macromol.* **2023**, *253*, 126851. [CrossRef]
36. Herrera, R.; Franco, L.; Rodríguez-Galán, A.; Puiggalí, J. Characterization and degradation behavior of poly(butylene adipate-*co*-terephthalate)s. *J. Polym. Sci. A Polym. Chem.* **2002**, *40*, 4141–4157. [CrossRef]
37. Kaboorani, A.; Riedl, B. Surface modification of cellulose nanocrystals (CNC) by a cationic surfactant. *Ind. Crops Prod.* **2015**, *65*, 45–55. [CrossRef]
38. Thakur, M.; Sharma, A.; Ahlawat, V.; Bhattacharya, M.; Goswami, S. Process optimization for the production of cellulose nanocrystals from rice straw derived α-cellulose. *Mater. Sci. Energy Technol.* **2020**, *3*, 328–334. [CrossRef]
39. Abraham, E.; Kam, D.; Nevo, Y.; Slattegard, R.; Rivkin, A.; Lapidot, S.; Shoseyov, O. Highly Modified Cellulose Nanocrystals and Formation of Epoxy-Nanocrystalline Cellulose (CNC) Nanocomposites. *ACS Appl. Mater. Interfaces* **2016**, *8*, 28086–28095. [CrossRef] [PubMed]
40. Siddiqui, M.N.; Redhwi, H.H.; Tsagkalias, I.; Softas, C.; Ioannidou, M.D.; Achilias, D.S. Synthesis and characterization of poly(2-hydroxyethyl methacrylate)/silver hydrogel nanocomposites prepared via in situ radical polymerization. *Thermochim. Acta* **2016**, *643*, 53–64. [CrossRef]
41. Tabatabaee, S.; Baheiraei, N.; Salehnia, M. Fabrication and characterization of PHEMA–gelatin scaffold enriched with graphene oxide for bone tissue engineering. *J. Orthop. Surg. Res.* **2022**, *17*, 216. [CrossRef]
42. Xue, D.; Wang, X.; Ni, H.; Zhang, W.; Xue, G. Surface Segregation of Fluorinated Moieties on Random Copolymer Films Controlled by Random-Coil Conformation of Polymer Chains in Solution. *Langmuir* **2009**, *25*, 2248–2257. [CrossRef] [PubMed]
43. Lettow, J.H.; Yang, H.; Nealey, P.F.; Rowan, S.J. Effect of Graft Molecular Weight and Density on the Mechanical Properties of Polystyrene-Grafted Cellulose Nanocrystal Films. *Macromolecules* **2021**, *54*, 10594–10604. [CrossRef]
44. Wu, Q.; Xu, J.; Wu, Z.; Zhu, S.; Gao, Y.; Shi, C. The effect of surface modification on chemical and crystalline structure of the cellulose III nanocrystals. *Carbohydr. Polym.* **2020**, *235*, 115962. [CrossRef]
45. Yoshikawa, C.; Qiu, J.; Huang, C.F.; Shimizu, Y.; Suzuki, J.; van den Bosch, E. Non-biofouling property of well-defined concentrated polymer brushes. *Colloids Surf. B Biointerfaces* **2015**, *127*, 213–220. [CrossRef]
46. Han, J.; Zhou, C.; Wu, Y.; Liu, F.; Wu, Q. Self-Assembling Behavior of Cellulose Nanoparticles during Freeze-Drying: Effect of Suspension Concentration, Particle Size, Crystal Structure, and Surface Charge. *Biomacromolecules* **2013**, *14*, 1529–1540. [CrossRef]
47. Roeder, R.D.; Garcia-Valdez, O.; Whitney, R.A.; Champagne, P.; Cunningham, M.F. Graft modification of cellulose nanocrystals via nitroxide-mediated polymerisation. *Polym. Chem.* **2016**, *7*, 6383–6390. [CrossRef]
48. Alamgir Md Mallick, A.; Nayak, G.C. Mechanical and thermal behavior of pHEMA and pHEMA nanocomposites targeting for dental materials. *Appl. Nanosci.* **2021**, *11*, 1257–1265. [CrossRef]
49. Leszczyńska, A.; Radzik, P.; Szefer, E.; Mičušík, M.; Omastová, M.; Pielichowski, K. Surface Modification of Cellulose Nanocrystals with Succinic Anhydride. *Polymers* **2019**, *11*, 866. [CrossRef]
50. Macke, N.; Hemmingsen, C.M.; Rowan, S.J. The effect of polymer grafting on the mechanical properties of PEG -grafted cellulose nanocrystals in poly(lactic acid). *J. Polym. Sci.* **2022**, *60*, 3318–3330. [CrossRef]
51. Zheng, T.; Clemons, C.M.; Pilla, S. Grafting PEG on cellulose nanocrystals via polydopamine chemistry and the effects of PEG graft length on the mechanical performance of composite film. *Carbohydr. Polym.* **2021**, *271*, 118405. [CrossRef] [PubMed]
52. Khoshkava, V.; Kamal, M.R. Effect of Cellulose Nanocrystals (CNC) Particle Morphology on Dispersion and Rheological and Mechanical Properties of Polypropylene/CNC Nanocomposites. *ACS Appl. Mater. Interfaces* **2014**, *6*, 8146–8157. [CrossRef] [PubMed]
53. Vatansever, E.; Arslan, D.; Sarul, D.S.; Kahraman, Y.; Gunes, G.; Durmus, A.; Nofar, M. Development of CNC-reinforced PBAT nanocomposites with reduced percolation threshold: A comparative study on the preparation method. *J. Mater. Sci.* **2020**, *55*, 15523–15537. [CrossRef]

Disclaimer/Publisher's Note: The statements, opinions and data contained in all publications are solely those of the individual author(s) and contributor(s) and not of MDPI and/or the editor(s). MDPI and/or the editor(s) disclaim responsibility for any injury to people or property resulting from any ideas, methods, instructions or products referred to in the content.